

Interpretation and Analysis of Potential Fluidized Landslide Slope

H. M. Shu¹, T. C. Chen^{2*}, W. C. Yang³ and Y. X. Luo⁴

¹Doctoral Student, Department of Civil Engineering, National Pingtung University of Science and Technology, Pingtung 912, Taiwan.

²Associate Professor, Department of Soil and Water Conservation, National Pingtung University of Science and Technology, Pingtung 912, Taiwan.

³Master, Department of Soil and Water Conservation, National Pingtung University of Science and Technology, Pingtung 912, Taiwan.

⁴Master student, Department of Soil and Water Conservation, National Pingtung University of Science and Technology, Pingtung 912, Taiwan.

¹E-mail: hung-ming@mail.swcb.gov.tw

²E-mail: tcchen@mail.npust.edu.tw

³E-mail: czero7961@gmail.com

⁴E-mail: redrose40262@gmail.com

ABSTRACT: Fluidized landslide, also called hillslope-type debris flow, often occurs on the village side hillslope in the mountain area during extreme weather condition. Fluidized landslide induces more severe damages than the shallow landslide; however its recognition model is still lacked. In this research a recognition model of the potential fluidized landslide slope was developed using 80 cases occurred in the Kaoping River basin, southern Taiwan. 30 fluidized landslides and 30 shallow landslides are employed for the model development and another 10 events of each landslide are applied for verification. Results show that the recognition model composed of 8 discriminant factors including geomorphology factors, hydrology factors and potential landslide factor predicated by SHALSTAB model provides accuracy rate of 85% of the verification events. Thus the model can be of practical use for fluidized landslide interpretation. The model can be used to identify the potential dangerous slope areas and effectively assist the disaster prevention and early warning of villages in mountain area.

KEYWORDS: Fluidized landslide, Discriminant analysis, Recognition model, SHALSTAB

1. INTRODUCTION

In 2009, Typhoon Morakot invaded Taiwan and caused many landslide-related disasters in the mountain areas of central and southern Taiwan. One of the serious hazardous area located at the river bank of Kaoping River basin, the fluidized landslides (FL) occurred on village neighbouring hillslopes claimed many casualties and losses. Taiwan is located at the boundary of the Eurasian Plate and the Philippine Sea Plates with dense faults and folds, complex geological structures, and frequent earthquakes. Situated in the subtropical area, Taiwan frequently experiences typhoons and heavy rainfalls lead to strong river incision and form steep and short river rapids. Over-development of hillside also results in disasters and the gradual increase of landslide incidences. Fluidized landslide often appears on the village neighbouring hillslope in the mountain area during extreme weather condition. The fluidized landslide induces more severe damages than the shallow landslide does. Residents live in the potential dangerous terrain without realizing it are subjected to great risk of safety.

Fluidized landslide also called hillslope-type debris flow (HDF) as shown in Figure 1 is smaller in scale when compared with the common stream-type debris flow. In terms of terrain, fluidized landslide slope (FLS) may not show apparent feature differences with erosion gully and shallow landslide (SL). In the recent literature (Evans, 1982; Hungr et al., 2001; Shieh, 2001; Lin, et al., 2002; Chou, 2002; Ho, 2003; Chen et al., 2004; Lu and Hsu, 2004; Benda et al., 2005; Jakob and Hungr, 2005; Wang, 2005; Yu et al., 2005; Jomelli et al, 2007; Chen et al., 2015), scholars focused more on characteristics of the terrain, occurrence, and mechanism of fluidized landslide, however, it still lacks the discriminant model of fluidized landslide and shallow landslide.

When Fluidized landslide occurs, the steep gradient causes faster flow and the short distance flow often impacts the settlements or houses below directly, so the warning time is relatively shorter. For disaster prevention, a terrain recognition model of fluidized landslide and shallow landslide is developed in this research, which can better identify dangerous slope areas, enhance the risk

assessment, and effectively assist the disaster prevention and early warning of villages in mountain area.

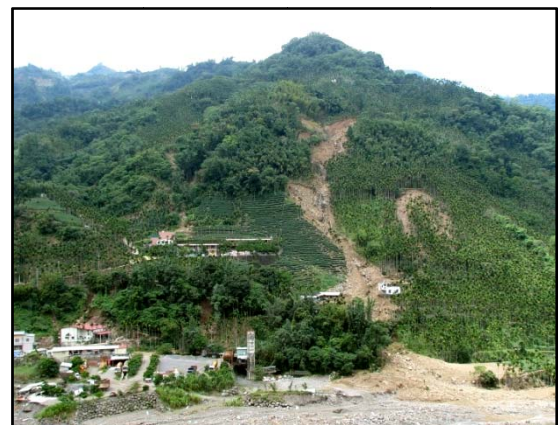


Figure 1 Two fluidized landslide events occurred in 2009 Typhoon

2. STUDY AREA-THE KAOPING RIVER BASIN

Kaoping River is a major river in southern Taiwan. The river originates near Yushan mountain (EL. 3,952m) as shown in Figure 2. The river flows through a series of rugged canyons and then is effluents into the Taiwan Strait. The length of this river is 171 kilometres and is draining a rugged area on the western side of the Central Mountain Range. Almost half of the basin has an elevation greater than 1,000 m. Only about 20 percent of the basin elevation is lower than 100 metres. The highest elevation of the watershed is located in the northeast region and then descends along the mountain ridge to the southwest region. Kaoping River is the second largest of Taiwan’s rivers by volume, with an average annual discharge of 8.45 km³/year.

The Chaozhou Fault divides the basin into two geological regions (Central Geological Survey, 2009), the strata in west of the fault is the sedimentary rock mainly included sandstone, siltstone, shale and mudstone. The main strata in east of the watershed is the Chaozhou formation (Co), this formation belongs to a class of Miocene sub-metamorphic rocks, with the majority of which consists of slate and phyllite as well as dark gray quartz sandstones with thickness of over 1000m around this area.

2. FACTORS OF THE RECOGNITION MODEL

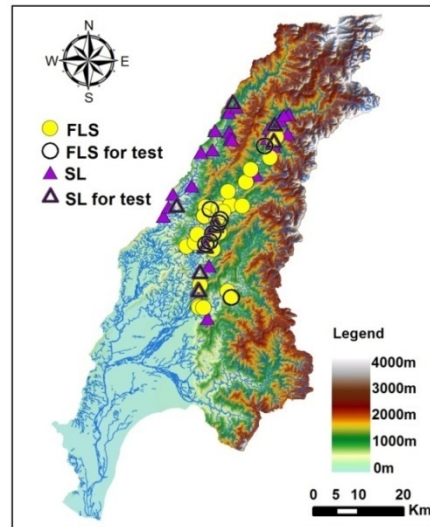
2.1 Map and database

The occurrence and location of fluidized landslide and shallow landslide are confirmed by aerial photographs, satellite images, landslide map after typhoon, 1/25000 terrain map, field investigation report, and hazard report. This study only selected the new fluidized landslide events, based on characteristics of hillslope debris flow developed by Chen et al. (2015), to extract the good quality of topographic characteristic. The aerial photos before and after Morakot have been inspected carefully to ensure there are no significant landslide and channels and well vegetation in the catchment before the disaster. Fluidized landslide slopes and non-fluidized landslide slopes, 40 cases each, are screened out and delineate the catchment area as the distribution shown in Figure 2a. The non- fluidized landslide cases, defining as the slope unit prone to shallow landslide but no fluidized landslide, are randomly delineated the slopes with the similar topographic nature around the fluidized landslide slopes which are inspected without debris flow transportation and accumulation after the disaster. From the aforementioned 80 entries, this study randomly select FLS and LS, 30 each, to develop a database for the recognition model, and the remaining, 10 each, data is retained as the validation for the effectiveness of the model.

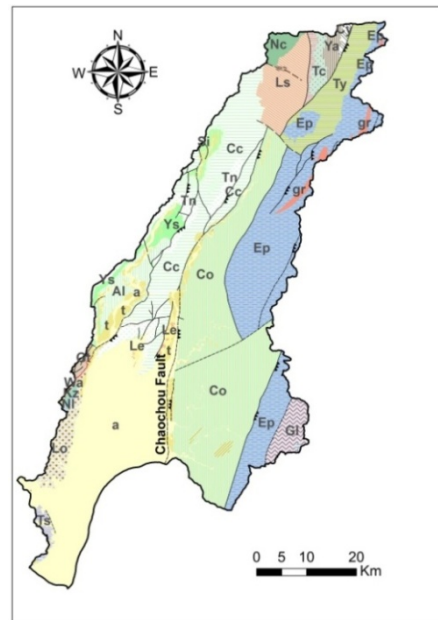
A geographical information system(GIS) platform was constructed for the data including the basin geological map, satellite images and aerial photos, landslide inventory of Typhoon Morakot, 5x5 m digital elevation model before and after the typhoon, and field survey on the local topography of landslide such as initiation, transportation, and deposition area. A total of 19 characteristic factors, such as topography, watershed, hydrology and other characteristics are developed for fluidized landslide slope interpretation as shown in Table 1.

2.2 Database of discriminate analysis

The recognition model composes of geological, geomorphological, and hydraulic factors. This study derived the factors using geographic information of the basin.



(a) Topographic map and location of study events



(b) geological map, (detail in the notes)

Note 1: sedimentary rock, a:Gravel, sand and mud, Al: Thin alternation of siltstone and shale, Cc: Alternation of sandstone and shale, Gt:Mud with intercalated sandstone, Hh: Thick-bedded siltstone, Kz: shale, Le: Conglomerate, sandstone, sandy shale and mudstone, Lo: Conglomerate with mudstone interbeds, Nc: sandstone and shale, Ni: Thick sandstone, mudstone, and shale, Si: Shale with siltstone, t: Gravel, sand, silt, and clay, Tn: Thick-bedded massive sandstone and muddy sandstone, Ts: Thick mudstone with sandstone and conglomerate interbeds, Ys: Massive shale,.

Note 2: Sub metamorphic rock, br: Basaltic pyroclastic rock, Ls: Slate, tu: Igneous rock, Co: Argillite and slate, Cu: Thick-layered marble, Cy: Slate with thin bedded siltstone, Ep:Slate with meta-sandstone and igneous rock, Gt: quartz-mica schist, gr: meta-igneous rock, Tc: sandstone, argillite and slate, Ty: Slate and phyllite, Ya: Quartzitic sandstone, argillite.

Figure 2 The topographic and geological (Central Geological Survey, 2009) maps of Kaoping River Basin. Locations of FLS and SL events are also showed in the topographic map

Table 1 Code table of the factors used for discriminant analysis

No	Characteristics factors	Codes
1	Watershed area	WA
2	Effective watershed area index	EWAI
3	Length of the transport segment	LT
4	Average width of the initiation region	AWI
5	Average width of watershed	AW
6	Average gradient of watershed	AGW
7	Average gradient of the initiation region	AGI
8	Gradient ratio of the initiation region	GRIR
9	Form factor of the initiation region	FFI
10	Form factor ratio	FFR
11	Elevation difference of pass ratio	EDPR
12	Elevation differences of the transport segment	EDT
13	Channel gradient of the initiation segment	CGI
14	Channel gradient of the transport segment	CGT
15	Depression ratio of the initiation segment ¹	DRI
16	Depression ratio of the transport segment ²	DRT
17	Ratio of landslide susceptibility area	RLSA
18	Landslide susceptibility area	LSA
19	Prediction ratio of shallow landslide ³	QT

¹ Depression ratio of the initiation segment (DRI) represents the concave nature of headwater hollow, the debris flow occurrence area, the depression ratio defined as the depth divided by the width of hollow.

² Depression ratio of the initiation segment (DRT) represents the concave nature of the transport channel area, the depression ratio defined as the depth divided by the width of channel below the pass point.

³ Area percentage of specified Q/T value range predicted by SHALSTAB

2.2.1 Watershed area and effective watershed area index

Watershed area (WA) is determined based on pre-disaster DEM to delineate the coverage area of watershed by GIS analysis. After the coverage is established, artificial contour line, satellite images and aerial photos are incorporated to revise the watershed boundary. Effective watershed area (EWA) which is the initiation region of the debris flow is defined as the drainage area below the ridge line and above the pass where the terrain reduces into a catchment as illustrated in Figure 3. In addition, the ratio of effective watershed area and the watershed area is defined as the effective watershed area index (EWAI).

The relationship between WA and EWAI of FLS and LS are shown in Figure 4. Figure 4 shows that there is no significant difference in sizes of EWA of FLS and LS, and the watershed area of FLS is larger than that of LS. As for the relationship between WA and EWAI, it appears that the EWAI of FLS is smaller while the EWAI of LS is larger. However, both EWAI decrease as WA increase, and two sets of data slightly show signs of clustering.

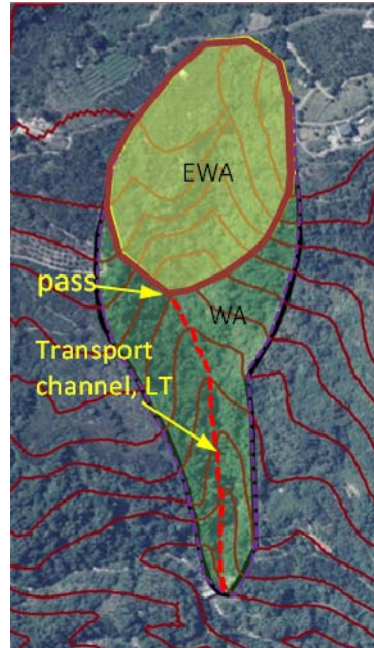


Figure 3 Illustrations of the watershed, pass, initiation area, and transport channel

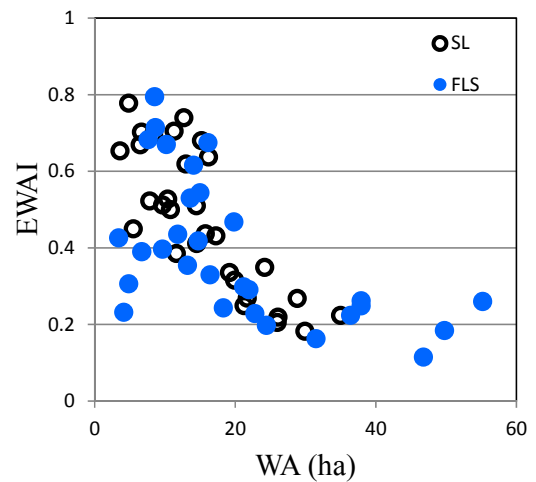


Figure 4 Distribution of watershed area, WA, and Effective watershed area index, EWAI

2.2.2 Length of the watershed and length of transport segment

The length of river channel mapped out by the geographical information system is generated by applying the orthographic projection concept. This study can calculate the actual slope distance (L_w) by $L/\cos\theta_f$ as shown in Figure 5, where L is the horizontal projected distance of the flow length (in m) and θ_f is the average slope gradient of the flow section (in degree). In the same way, this study can determine the length of transport segment (LT) by $L_t/\cos\theta_f$. Figure 6 shows the relationship between the length of transport segment and watershed area of FLS and SL, the length of watershed is dependent of watershed area, when the watershed area increases, the length of transport segment also increases. Figure 6 shows that there is no significant difference in LT of FLS and LS, except the LT and WA of FLS is larger than those of SL.

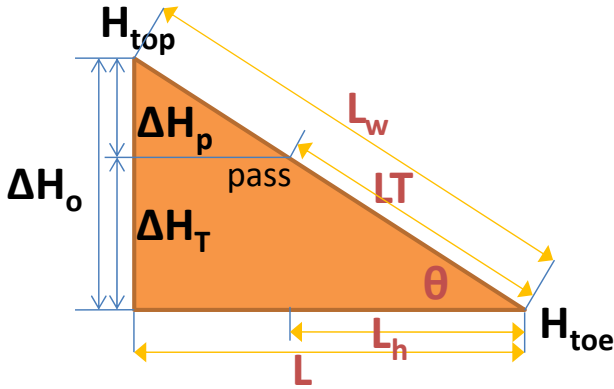


Figure 5 Schematic diagram of the dimensions of a watershed

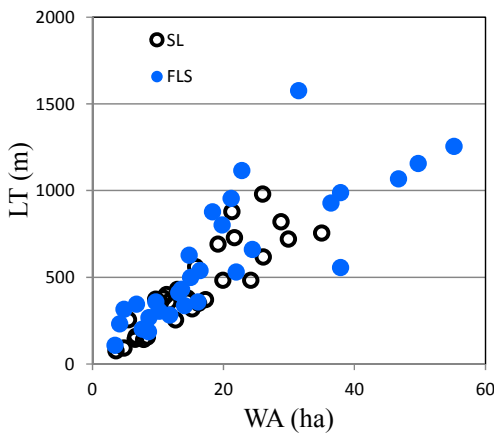


Figure 6 Distribution of length of the transport segment LT and watershed area WA

2.2.3 Average width of watershed and average width of the initiation region

This study derive the watershed area and the length of the watershed by GIS tool, and divide WA by L_w to obtain the average width of the watershed (AW). The average width of the initiation segment (AWI) is also obtained by the above method. The initiation area is the source to debris flow and the shape of the initiation region can further indicate the debris production of that area. Figure 7 shows the distribution of average width of watershed AW and average width of the initiation segment AWI; however there is no significant difference in AWI of FLS and LS.

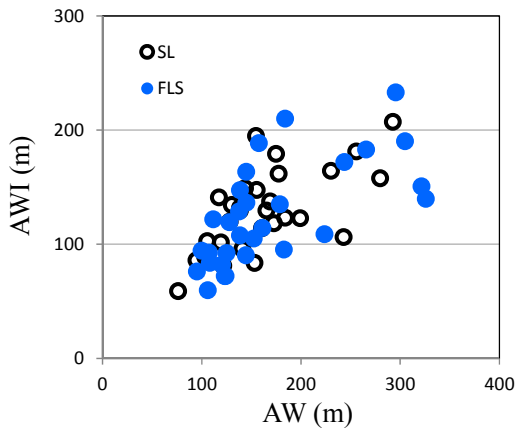


Figure 7 Distribution of average width of watershed AW and average width of the initiation segment AWI

2.2.4 Average gradient and gradient ratio of the initiation region

This study use GIS to calculate the average gradient of the watershed (AGW) and average gradient of the initiation region (AGI) via the digital elevation model and further obtain the gradient ratio of the initiation region (GRIR) by dividing AGI by AGW. This study explores the distribution of AGW, AGI, and GRIR of FLS and LS, and the results are shown with the relationship between the two factors in Figure 8 and 9. In Figure 8, this study can see that the distributions of AGW and AGI are more dispersed (the average gradient of watershed distributes between 18° and 45° , and about the same as the initiation location) and are more concentrated along a slope line and both factors show a direct proportion. As for FLS, the distribution is more concentrated (between 25° and 40° for watershed and between 20° and 38° for initiation location) and the two factors show in proportion. Next, this study compare the AGW with GRIR (Figure 9) and find that the GRIR of LS is about 1, indicating that the change of overall watershed is mild. For FLS, the distribution is more dispersed, indicating that the overall gradient change is more significant.

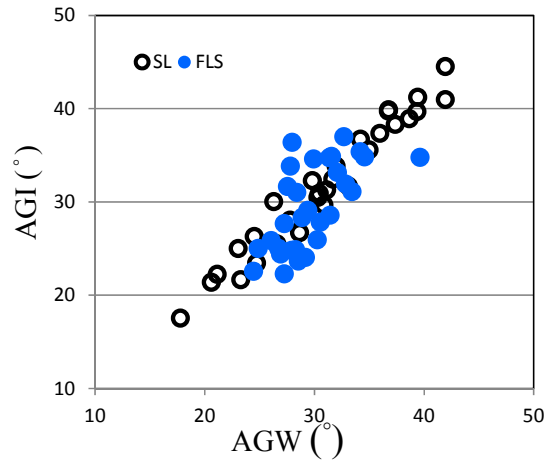


Figure 8 Distribution of average gradient of watershed AGW and average gradient of the initiation region AGI

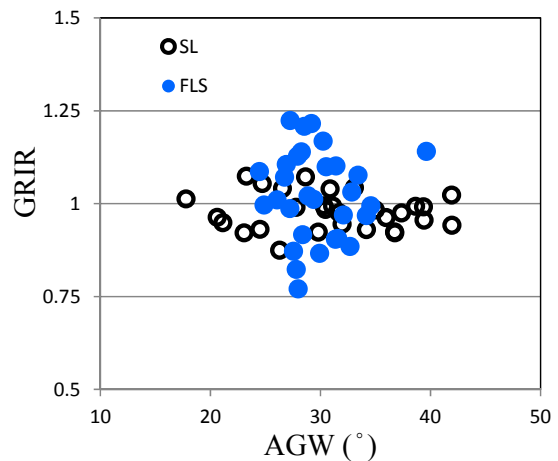


Figure 9 Distribution of average gradient of watershed AGW and gradient ratio of the initiation region GRIR

2.2.5 Form factor of the initiation region and Form factor ratio

Form Factor of watershed was raised by Horton (1932) and defined as: form factor $F = WA/L_w^2$, where L_w is the length of the main stream; WA is the watershed area; the form factor represents watershed area per main stream length, large form factor represents wider watershed and vice versa. This study define the form factor of

the initiation region (FFI) as EWA divided by the length of initiation segment, and Form factor ratio $FFR = FFI/F$. Figure 10 shows the distribution of FFI and FFR, it is found that the form factors were mostly distributed between 0.2 to 0.6. Despite, the watersheds were in long and narrow shape, the initiation region appears more rounded shape than whole watershed since the FFRs are larger than 1.

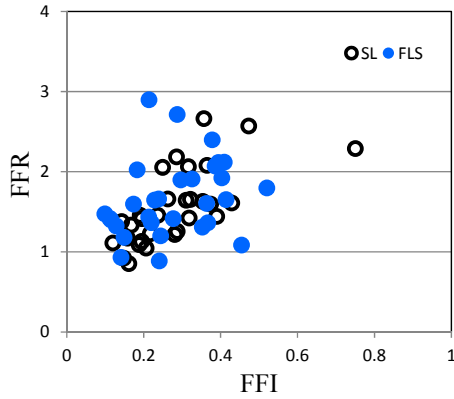


Figure 10 Distribution of Form factor of the initiation region FFI and form factor ratio FFR

2.2.6 Elevation difference of pass ratio and elevation differences of the transport segment

This study obtain elevation difference of pass ratio (EDPR) by dividing the elevation difference of initiation region by the elevation difference of watershed. The ratio represents the location of initiation on the watershed profile. The larger the value is, the closer the pass is to the slope toe, and the smaller the value is, the closer the pass is to the section between the mid-section and the top of slope. Elevation differences of the transport segment (EDT) means the elevation differences between the pass and the deposition. This study further explore EDPR and EDT of FLS and LS and the distribution is as shown in Figure 11. Figure 11 shows that LS distribution is more concentrated and FLS is more dispersed. EDPR and EDT show that they are roughly in proportion with a linear relationship. The distribution for FLS is slightly more dispersed and EDT for FLS is larger than that of LS.

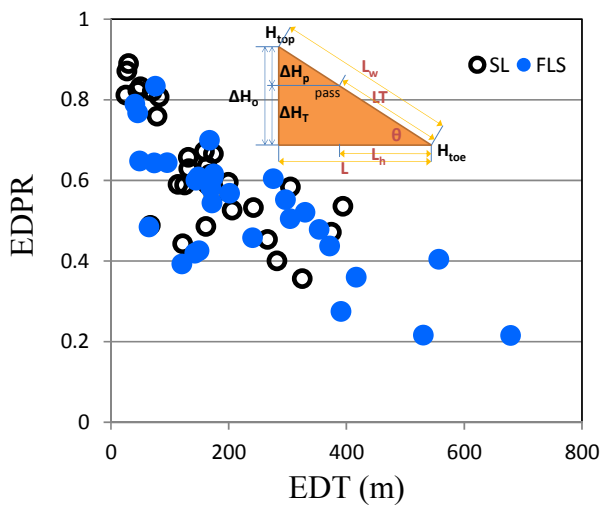


Figure 11 The distribution of elevation difference of pass ratio EDPR and elevation differences of the transport segment EDT

2.2.7 Channel gradient of watershed and transport segment

On the channel profile aspect, this study produces channel gradient of segments, which are for the initiation segment (CGI) and the transport segment (CGT), to further explore the longitudinal profile and terrain changes of the whole watershed. After producing the differences in height (ΔH) and horizontal distance (L) as shown in Figure 5, the difference in height (ΔH) is divided by the horizontal distance (L) to obtain the gradient of channel. The distributions of EDT and CGI of FLS and LS are shown in Figure 12. EDTs and CGIs for LS are more concentrated with a linear trend and the two factors show an increasing proportion. As for FLS, the distribution is more dispersed and the two factors are in an increasing proportion but the correlation is not so significant.

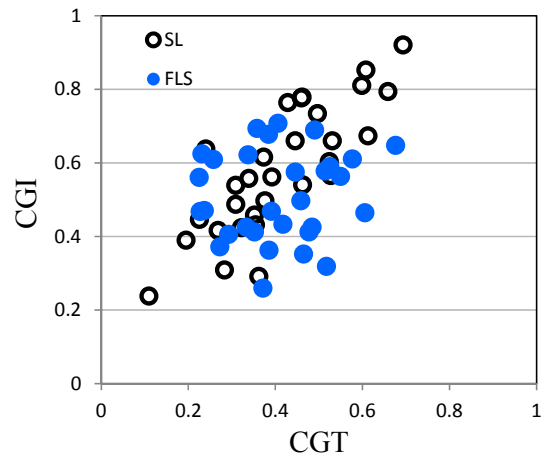


Figure 12 The distribution of channel gradient of the initiation segment CGI and channel gradient of the transport segment CGT

2.2.8 Depression ratio of the initiation and transport segments

In cross-section aspect of the watershed, this study divides it into two regions, Depression ratio of the initiation segment (DRI) to represents the concave nature of headwater hollow, the debris flow occurrence area, and Depression ratio of the transport segment (DRT), to further explore the cross-section and terrain changes of the watershed. To obtain the depression ratio, the Japan's National Institute for Land and Infrastructure Management (2007) is referred as shown in Figure 13. A 1/25,000 topographic map is used to obtain the width of the whole, initiation, and transport segment as the width, a , and the depth, b , and b is divided by a to obtain the depression ratio. The distributions of depression ratios of DRI and DRT of FLS and LS are shown in Figure 14. The results in Figure 14 show that the terrain changes of LS are not as apparent as that of FLS, which indicates that the FLS watershed has more incision in the transport segment.

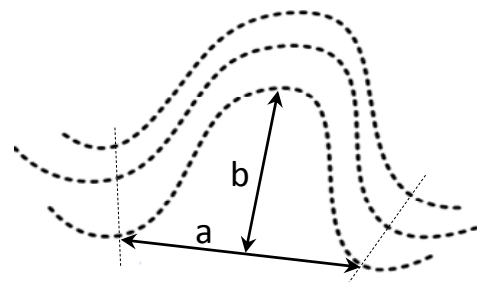


Figure 13 The schematic diagram of the width, a , and depth, b , of torrent (Japanese National Institute for land and infrastructure management, 2007)

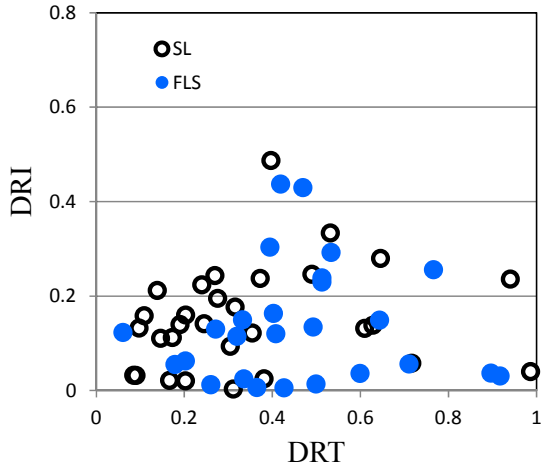


Figure 14 Distribution of depression ratio of the initiation segment DRI and depression ratio of the transport segment DRT

2.2.9 Landslide susceptibility area ratio

The ratio of landslide susceptibility area developed by Chen (2013) is used in model. It is obtained by dividing the landslide susceptibility area (LSA) by the watershed area (WA). The bigger the ratio of landslide susceptibility area is, the wider the landslide coverage of the region is, or vice versa.

According to the previous landslide susceptibility area study, the landslide mainly occurs between slope angle of 18 to 45 degrees. This study calculate the average number of cells of every gradient for FLS and LS, and Figure 15 represents the average number of cells of landslide susceptibility area of the two types of landslides. This figure shows that the landslide susceptibility area mainly distributes between 20 and 44 degree, which is somewhat consistent with the previous findings. This study take the gradient of 1 degree (decimal rounding) and differentiate, and the attempted results are shown in Figure 16. This study can see that for the slope gradients between 30 and 35 degree, there are significant differences. This study therefore takes the generated LSA and RLSA as effective factors.

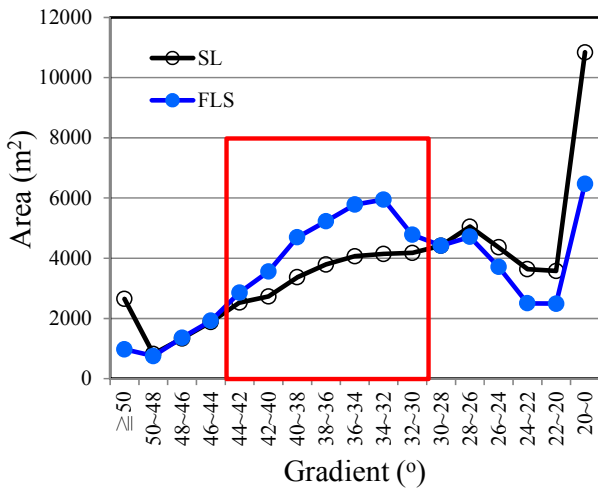


Figure 15 Distribution of landslide susceptibility slope area and the average number of cell

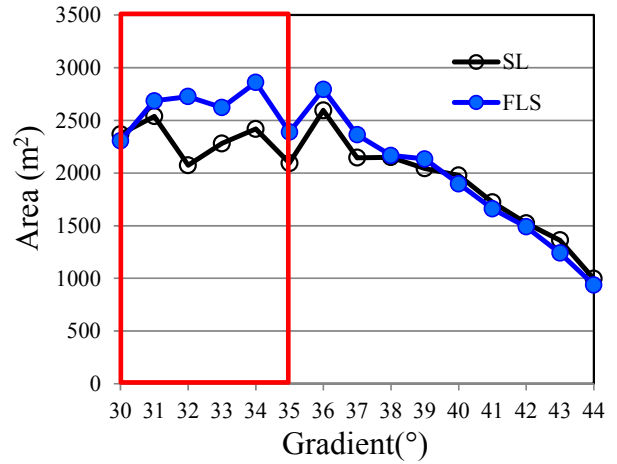


Figure 16 Distribution of landslide susceptibility slope gradient and the average number of cell

2.2.10 Prediction ratio of shallow landslide (QT)

This study adopts SHALSTAB (Dietrich and Montgomery, 1994) to perform the unstable slope coverage analysis and predicts the landslide coverage ratio as part of the factors. Based on key assumptions: Infinite inclined plane with angle θ , failure plane parallel to the surface, failure occurs at soil/bedrock boundary, and flow parallel to the failure boundary as shown in Figure 17, SHALSTAB model combined the slope stability model in the infinite slope condition and the hydrological model of ground water level in soil layer. Slope does not need to be fully saturated for failure, the critical state of stability of slope can be express as Eq.(1):

$$\frac{h}{z} = \frac{c'}{\gamma_w z \cos^2\theta \tan\phi'} + \frac{\gamma_{sat}}{\gamma_w} \left(1 - \frac{\tan\theta}{\tan\phi'}\right) \quad (1)$$

In above equation, z is the depth of soil; h is the height of ground water level from sliding surface; c' and ϕ' are the effective cohesion and friction angle of soil; γ_{sat} is unit weight of soil in saturation; γ_w is unit weight of water; and θ is infinite inclined plane angle.

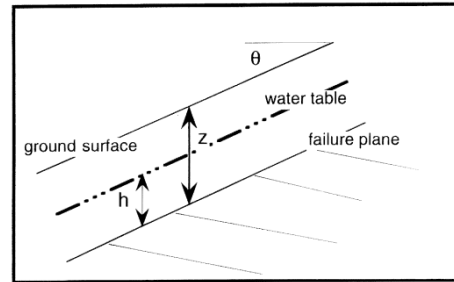


Figure 17 the schematic diagram of the assumption of SHALSTAB.

In steady state subsurface flow condition, shown in Figure 18, the total effective precipitation Qa fully transforms into the sub-ground flow:

$$Qa = k_s h b \sin\theta \cos\theta \quad (2)$$

The transmissivity is defined as the relationship:

$$T = k_s z \cos\theta \quad (3)$$

Then Eq.(4) is obtained as following.

$$\frac{h}{z} = \frac{Q}{T} \cdot \frac{a/b}{\sin\theta} \quad (4)$$

In above equation, Q: effective rainfall (p – ev - d), θ: surface slope, ks: the saturated conductivity, T: the transmissivity, a/b: drainage area per cell width, h/z: relative saturation.

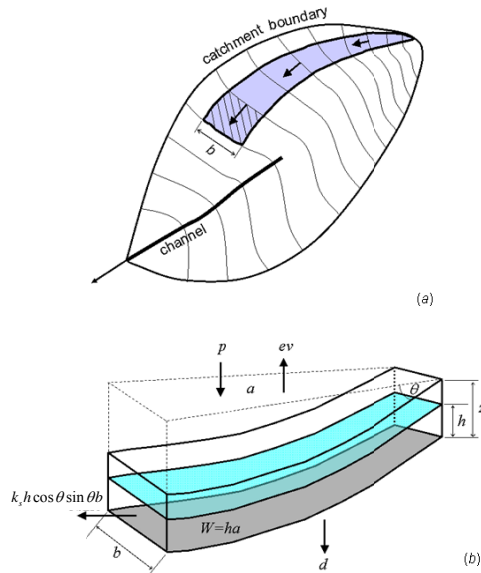


Figure 18 The schematic diagram of SHALSTAB model, a is the drainage area, b is the width of slope unit, d is the infiltration, ev is the evaporation, and p is the precipitation. (Dietrich and Montgomery, 1994)

The SHALSTAB model and various parameters is shown in Eq. (5) and Table 2, in which C, φ, b, γs, and γw are constants and θ, z, and a are variables, and the parameter configuration are shown in Table 1:

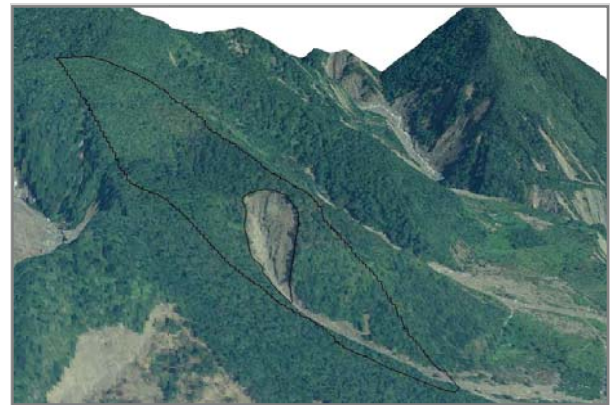
$$\frac{Q}{T} = \left\{ \frac{c'}{\gamma_w z \cos^2\theta \tan\theta'} + \frac{\gamma_{sat}}{\gamma_w} \left[1 - \frac{\tan\theta}{\tan\theta'} \right] \right\} \left[\frac{b \sin\theta}{a} \right] \quad (5)$$

Table 2 Parameter settings adopted by SHALSTAB model

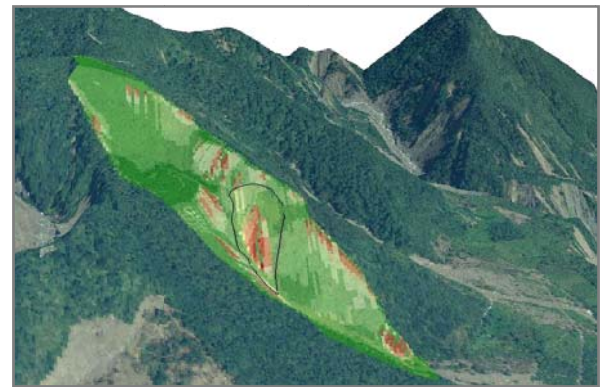
	Parameter	Value
Const ants	Mass density of water, γ _w (kN/m ³)	9.81
	Mass density of soil, γ _s (kN/m ³)	18
	Width, b (m)	5
	Metamorphic soil, cohesion C (kPa)	17.8
	Metamorphic soil, angle of friction φ (degree)	25
	Sedimentary soil, cohesion C (kPa)	11.7
Varia bles	Sedimentary soil, angle of friction φ (degree)	27.3
	Watershed area, a	Obtained from GIS
	Slope gradient, θ (degree)	Obtained from GIS
	Soil depth, Z (m)	Obtained from the slope gradient
	Elevation value, h (m)	Obtained from GIS

The Q/T value of every grid is obtained using the analysis of SHALSTAB model. If Q/T value is higher than 0, then the slope is more stable; if the value is less than 0, then the slope is not so stable. The unstable area may experience landslide and this can be regarded as the prediction to FLS. This study use GIS to obtain the elevation value (h) of every grid with the digital elevation model. Elevation value is the change in vertical component.

Terrain also requires a horizontal component and the value "a" can be used as the change in horizontal water flow. Both values a, and h used in a grid are considered as a changing parameters. By comparison with the Q/T value and the real landslide inventory, landslides mostly distributed with the Q/T values between -0.75 and -2 as illustrated in Figure 19. Therefore, this study takes Q/T area ratio by the area of Q/T values range from -0.75 to -2 divides by WA. Figure 20 shows the distribution of WA and Q/T which demonstrates the distribution of Q/T and WA is more dispersed for FLS, the Q/T ratio decrease till less than 10 % as the WA large than 40 ha. This means the potential landslide area is limit for a watershed. The case of SL is more concentrated with a down linear trend.



(a) Aerial photos after Typhoon Morakot (perspective view)



(b) Overlay of results from SHALSTAB analysis

Figure 19 Overlay of SHALSTAB analysis results and the aerial photos post-disaster (perspective view)

Q/T ratio is increasing with average gradient of watershed as shown in Figure 21. The distribution is concentrated within 20 to 35 degrees of average gradient of watershed for FLS, and SL is more disperse from AGW 20 to 45 degree. Both FLS and SL illustrate a linear trend on Q/T and AGW that means the large gradient of water possess potentially the high landslide probability. The depression of the initiation segment influences Q/T ratio of a watershed as shown in Figure 22, the small depression rate, more flat shape, take a disperse Q/T rate distribution, and the Q/T rate concentrated to 10% in the large DRI, more concave shape, for FLS. This means the

potential landslide area is dispersed on a flat shape side slope, however the potential landslide trends to a convergence to 10 % in the large depression headwater area.

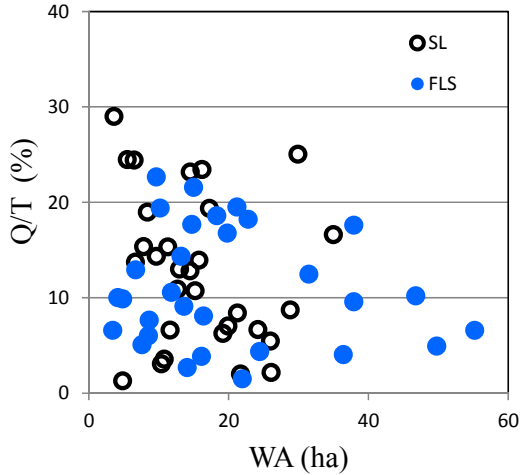


Figure 20 Distribution of watershed area WA and Q/T

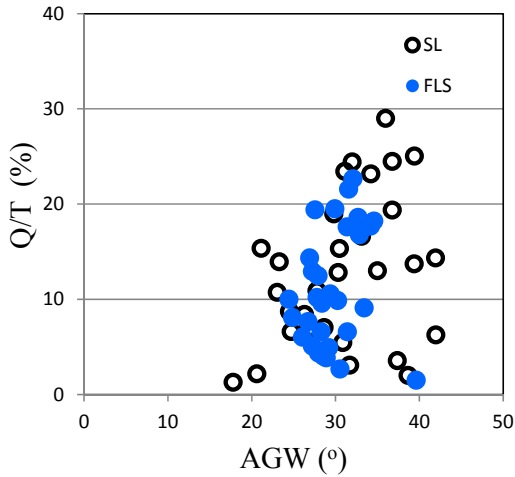


Figure 21 Distribution of average gradient of watersheds and Q/T

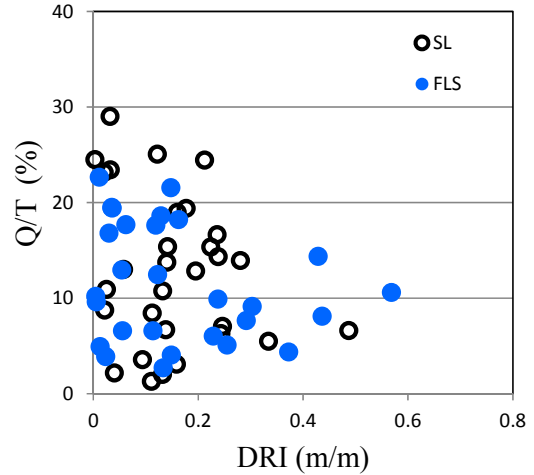


Figure 22 Distribution of depression of initiation segment and Q/T

3. DISCRIMINANT ANALYSIS RESULTS AND DISCUSSIONS

This study uses discriminant analysis to establish a determination model for FLS. The discriminant analysis adopts 20 factors to conduct stepwise selection based on the estimation rate between the discriminant factors of each group. Eight best factors were adopted and an analysis model for fluidized landslide slope susceptibility was obtained. The model then uses the additional 10 sets of FLS and LS cases as the validation sample groups and performs prediction tests based on the discriminate functions from the results of discriminant analysis.

3.1 Combinations and results of variables in the discriminant analysis

This study adopts SPSS to conduct discriminant analysis. To keep the sampling probability of the two populations, fluidized landslide slope and shallow landslide slope, the same, 30 events are selected from each population for a total of 60 samples. This study selects a total of 19 factors among the geological and shallow layer landslide factors as predictors to conduct discriminant analysis. The factor combination and the estimation rate for discriminant analysis are shown in Table 3.

Table 3 Factors combinations and estimation rate of discriminant analysis

Factor combination	Estimation rate
EWA+EWAI+EDT+EDPR+CGT+LT+FFI+FFR+AW+AWI+DRI+DRT+CGI+AGW+AGI+GRIR+LSA+RLSA+QT	88.3%
EWAI+EDT+EDPR+CGT+LT+FFI+FFR+AW+AWI+DRI+DRT+CGI+AGW+AGI+GRIR+LSA+RLSA+QT	88.3%
EWAI+EDPR+CGT+LT+FFI+FFR+AW+AWI+DRI+DRT+CGI+AGW+AGI+GRIR+LSA+RLSA+QT	88.3%
EWAI+EDPR+CGT+LT+FFR+AW+AWI+DRI+DRT+CGI+AGW+AGI+GRIR+LSA+RLSA+QT	86.7%
EWAI+EDPR+CGT+LT+FFR+AWI+DRI+DRT+CGI+AGW+AGI+GRIR+LSA+RLSA+QT	86.7%
EWAI+EDPR+CGT+LT+FFR+AWI+DRT+AGIC+AGW+AGI+GRIR+LSA+RLSA+QT	86.7%
EWAI+EDPR+CGT+LT+FFR+AWI+DRT+AGW+AGI+GRIR+LSA+RLSA+QT	86.7%
EWAI+EDPR+CGT+LT+FFR+AWI+DRT+GRIR+LSA+RLSA+QT	85.0%
EWAI+EDPR+CGT+LT+FFR+AWI+DRT+GRIR+LSA+QT	85.0%
EWAI+CGT+LT+FFR+AWI+DRT+GRIR+LSA+QT	85.0%
EWAI+CGT+FFR+AWI+DRT+GRIR+LSA+QT	90.0%

This study input the data of 19 characteristic factors into SPSS for discriminant analysis and selects the optimum factor combination to obtain a standardized discriminant function. The effectiveness of factor have been shown in Table 3, the estimation rate is 88.3 % for overall 19 factors combination. Then, the combination for 18 factors from eliminating one by one factor obtained the best estimation rate is 88.3 % and same result on 17 factors combination. Table 3 shows the combination of 19, 18, 17, 16, 15, 14, 13, 11, 10, 9, and 8 factors results the best estimation rate in 88.3, 86.7, 85.0, and 90.0 %. The highest estimation rate among the combinations composed of 9 factors. The optimum factor combination to obtain a standardized discriminant function as shown below:

$$y=0.286X_1+0.739X_2-0.280X_3-1.259X_4-0.226X_5+0.796X_6+1.152X_7-0.139X_8 \quad (6)$$

In above equation, y is the discriminant function, X₁ is the form factor ratio FFR, X₂ is the gradient ratio of the initiation region GRIR, X₃ is the effective watershed area index EWAI, X₄ is average width of the initiation region AWI, X₅ is the channel gradient of the transport segment CGT, X₆ is the depression ratio of the initiation segment DRT, X₇ is the landslide susceptibility area LSA, and X₈ is Prediction ratio of shallow landslide Q/T.

When the coefficient of the discriminant function is negative, the factor is inversely proportional to the linear function of discriminant analysis, namely: EWAI, AWI, CGT and Q/T percentage which are negatively correlated with the discriminant model. On the other hand, factors such as FFR, GRIR, DRT and LSA are positively correlated with the determinant model. If the discriminant function y is greater than 0, a fluidized landslide slope is identified, otherwise a shallow landslide slope is identified. The results are shown in Table 4, in which the overall correct estimation rate is 90.0%. The impact factors are determined as having low degree of correlation after going through correlation test (Table 5), meaning that each factor is independent and does not affect each other.

Table 4 Analysis results from discriminant analysis

		Original Prediction		Total %
Result	Item	FLS	LS	
Number	FLS	27	3	30
	LS	3	27	30
Percentage (%)	FLS	90	10	100
	LS	10	90	100
Overall estimation rate = (27+27)/(30+30) × 100% = 90.0%				

Figure 23 shows the distribution of discriminant function of FLS and LS. The x-axis is the discriminant function and y-axis is the percentage in which the number of data accounts for the overall database. For FLS, the function value is in between -1.71 and 2.44. For LS, the function value is between -2.21 and 2.31. This study test the impact of each factor on the estimation rate and their coefficients of discriminant function are listed in Table 6. Among them, material factor impacts the estimation rate greatly, indicating that the prediction of landslide is extremely important to determine the fluidized landslide slope.

Table 5 Results showing the correlation of discriminant factors

Related matrix	FFR	HA SR	EW AI	AWI	CGT	HA RF	LSA	QT
FFR	1	0.23	-0.12	0.54	-0.07	0.11	0.14	-0.09
GRIR	0.23	1	-0.02	0.09	0.27	-0.09	-0.26	-0.30
EWAI	-0.12	-0.02	1	0.06	-0.05	-0.17	0.25	0.11
AWI	0.54	0.09	0.06	1	-0.29	0.31	0.54	-0.23
CGT	-0.07	0.27	-0.05	-0.29	1	-0.36	-0.04	0.18
DRT	0.11	-0.09	-0.17	0.31	-0.36	1	-0.08	-0.19
LSA	0.14	-0.26	0.25	0.54	-0.04	-0.08	1	0.11
QT	-0.09	-0.30	0.11	-0.23	0.18	-0.19	0.11	1

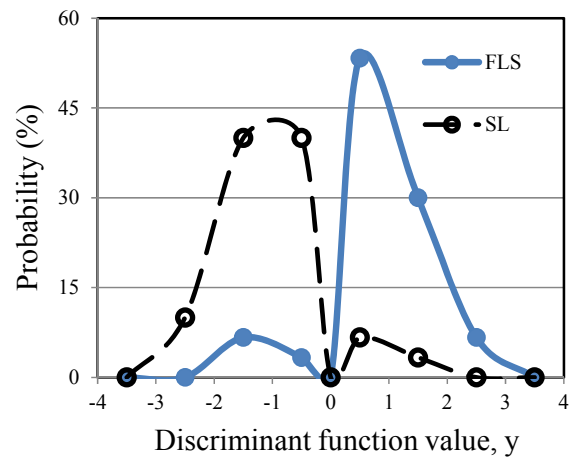


Figure 23 The distribution of discriminant function of FLS and LS.

Table 6 Impact of discriminant factors on the estimation rate

Item	Characteristics factors			Weighting (%)
	Coefficient of discriminant function			
Material factor	GRIR	LSA	QT	41.6
	0.739	1.152	0.139	
Terrain factor	DRT	CGT		20.9
	0.796	0.226		
Hydrology factor	EWAI	FFR	AWI	37.4
	0.280	0.286	1.259	

3.2 Validation of the discriminant model

The 10 sets of each event in the study area are taken as verification samples, with each from the watersheds of FLS and LS near the population samples.

This study generate 8 sets of data from the discriminant factors (form factor ratio, average slope gradient, effective watershed area index, average width of the initiation area, average slope gradient of hillslope, aspect ratio of hillslope, landslide susceptibility area and Q/T percentage) of the 20 verification points and applied to Eq. (6) to obtain the verification results shown in Figure 24 and Table 7. This study obtains the estimation rate of test samples is 85%. The result demonstrates that this fluidized landslide slope susceptibility model can effectively determine the probability of fluidized landslide in Kaoping River basin.

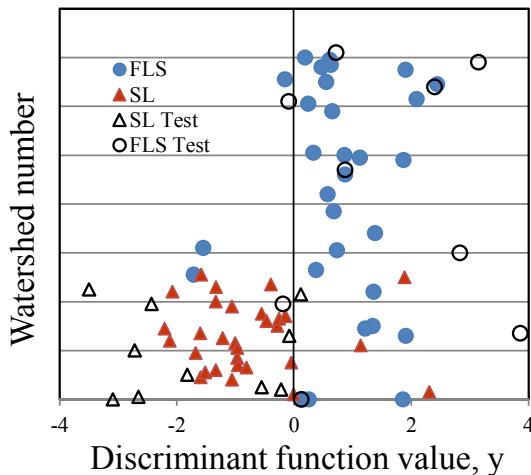


Figure 24 The distribution of verification locations and the population's discriminant function at FLS and LS

Table 7 Test results from discriminant analysis

		Original		Prediction		Total %
		FLS	LS	FLS	LS	
Number	FLS	8	2	8	2	10
	LS	1	9	1	9	10
Percentage (%)	FLS	80	20	80	20	100
	LS	10	90	10	90	100
Overall estimation rate = $(8+9)/(10+10) \times 100\% = 85.0\%$						

4. CONCLUSIONS

This study focused the fluidized landslide slopes at Kaoping River basin and selects 19 characteristics factors to develop a database based on three conditions contributing to debris flow, which are terrain factor, hydrological factor and material factor. This study use discriminant analysis to establish a estimation model for fluidized landslide slope susceptibility and conduct verification to explore the factors causing fluidized landslide at different locations. The results are summarized as follow:

1. Among the 19 characteristics factors analysed in this study, the form factor ratio, gradient ratio of the initiation region, effective watershed area index, average width of the initiation

region, channel gradient of the transport segment, depression ratio of the initiation segment, landslide susceptibility area, and Q/T percentage, a total of 8 factors, achieve the best estimation rate with the overall accuracy of 90% for fitting.

2. This study verified the fluidized landslide estimation model and draw out 10 cases each of the FLS and LS in the watersheds for prediction. The verification obtains an accuracy rate of 85%.
3. The model developed in the study can enhance the understanding of slope units with the relatively high susceptibility of fluidized landslide and could be used as reference for the risk assessment of slopes, which provides information for disaster prevention and early warning in advance.

5. REFERENCES

Benda, L., Hassan, M. A., Church, M., and May, C. L. (2005) "Geomorphology of Steepland Headwaters: The transition From Hillslopes to Channels." *Journal of the American Water Resources Association (JAWRA)* 41(4):835-851.

Central Geological Survey. (2009) Geological map of Kaoping River Watershed. Scale: 1:50,00.

Chen, B.L. (2013) Potential analysis and deposition characteristics of hillslope debris flows, Master Thesis, Dept. of soil and water conservation, National Pingtung university of science and technology. (in Chinese)

Chen, J.C., Shieh, C.L., Lin, C.W. (2004) "Topographic Properties of Debris Flow in Central Taiwan," *Journal of Chinese Soil and Water Conservation*, 35 (1):25-34. (in Chinese)

Chen T.C., Wang, Z.Y., and Chen B.L., 2015, "Geomorphological Nature and Identification of Hillslope Debris Flow," *Journal of Chinese Soil and Water Conservation*, 46 (3): 133-141. (in Chinese)

Chou, H.T. (2002) Slope Failure and Debris Flows Mobilization from Landslides (I), research report of National Science Council, NSC90-2625-z-008-006. (in Chinese)

Dietrich, W.E., and Montgomery, D.R. (1994) "A Physically Based Model for the Topographic Control on Shallow Landsliding," *Water Resources research*, Vol.30, No.4, pp. 1153-1171.

Evans, S. G., 1982, "Landslides and surficial deposits in urban area of British Columbia." *Canadian Geotechnical Journal*, 19, pp. 269-288

Ho, M.H. (2003) Failure Mechanism of Slope-Type debris flow in The Central Area of Taiwan, Master Thesis, Dept. of Civil engineering, National Taiwan University. (in Chinese)

Horton, H.E. (1932) "Drainage-basin Characteristics," *American Geophysical Union*, Vol.13, pp.350-61.

Hungr, O., Evans, S.G., Bovis, M. & Hutchinson, J.N. (2001) Review of the classification of landslides of the flow type. *Environmental and Engineering Geoscience* VII: 221-238.

Jakob, M., and Hungr, O. (2005) Debris-flow hazards and related phenomena, Springer, Berlin, New York, 170 p.

Jomelli, V., Brunstein, D., Grancher, D., and Pech, P. (2007) "Is the Response of Hill Slope Debris Flows to Recent Climate Change Univocal? A Case Study in the Massif Des Ecrins (French Alps)," *Climatic Change*, Vol. 85, pp.119-137.

Lin, C.W., Shieh, C.L., Wang, W.N. (2002) "Chi-Chi earthquake induced the landslide and debris flow in central Taiwan," Conference on Taiwan's active fault and earthquake hazard, Tainan, pp.124-134. (in Chinese)

Lu, K.K. and Hsu, M.L. (2004) "The Geomorphic Characteristics of Debris Flows in the Ninety-Nine Peaks Area, Nantou," *JOURNAL OF GEOGRAPHICAL SCIENCE* (38) : 1-16. (in Chinese)

National Institute for land and infrastructure management (2007) Manual of technical standard for establishing SABO master plan for debris flow and driftwood, Japan. (in Japanese).

Shieh, C.L. (2001) Potential analysis of debris flow in the affected area of Typhoon Toraji, research report of Soil and Water

- Conservation Bureau, Council of Agriculture, Executive Yuan. (in Chinese)
- Wang, L.C. (2005) The characteristics of topography and occurrence of hillslope debris flows in Shitou area., Master Thesis, Dept. of Earth Sciences, National Cheng Kung University. (in Chinese)
- Wang, Z.Y. (2012) The identification and topographic evolution of hillslope debris flows, Master Thesis, Dept. of soil and water conservation, National Pingtung university of science and technology. (in Chinese)
- Yu, F.C., Wu, J.M, and Wong, W.M. (2005) “Study on Micro-Geomorphological Features of Debris Flow on Hillslope of Conglomerate Formation,” *Journal of Soil and Water Conservation*, 37(4):329-340. (in Chinese)